SAND2020-5174C

**Proceedings of The ASME 2020 International Design Engineering Technical Conferences & Computers and Information in Engineering Conference**
**IDETC/CIE 2020**
**August 16-19, 2020, St. Louis, USA**

**IDETC2020-22417**

# SUBSTRUCTURE INTERFACE REDUCTION TECHNIQUES TO CAPTURE NONLINEARITIES IN BOLTED STRUCTURES

**Aabhas Singh**
Department of Engineering Physics
University of Wisconsin - Madison
Madison, WI, 53706
Email: singh36@wisc.edu

**Matthew S. Allen**
Department of Engineering Physics
University of Wisconsin - Madison
Madison, WI, 53706
Email: msallen@wisc.edu

**Robert J. Kuether**
Component Science and Mechanics
Sandia National Laboratories
Albuquerque, NM, 87123
Email: rjkueth@sandia.gov

## ABSTRACT

*In structural dynamics, a common practice when modeling bolted joint structures is to create finite element models (FEM) using multi-point constraints (MPC) and/or joint element(s) to reduce the number of DOF (Degrees of Freedom) that need to be joined at the contact interfaces. Scalability becomes an issue when multiple joints are present in a system, each requiring a nonlinear hysteretic model to capture the nonlinear behavior. While this increases the computational cost, the larger problem is that the parameters (and even the form) of the joint models are not known, and so one must solve a nonlinear model updating problem with hundreds of unknown variables to fit the model to measurements. Furthermore, traditional approaches are limited in how the flexibility of the interface is treated (i.e. with rigid bar elements the interface has no flexibility). To resolve this shortcoming, this work presents an alternative approach where the contact interface is reduced to a set of modal DOF which retain the flexibility of the interface and are capable of modeling multiple joints simultaneously while capturing the global dynamics of the structure. Specifically, system-level characteristic constraint (S-CC) reduction is used to reduce the contact interface to a small number of shapes that describe the global deformation. To capture hysteresis and energy dissipation that is present during microslip of joints, a hysteretic element is used for a small number of S-CC Shapes. This method is compared against a traditional MPC method constrained with rigid bar elements on a 2D cantilever beam structure with a single joint near the free end. For all methods, a four-parameter Iwan element is applied to the interface DOF to capture how the amplitude dependent modal frequency and damping change with vibration amplitude.*

## INTRODUCTION

Large structural finite element models are modeled with several sub-assemblies that are connected with joints and introduce mechanical interfaces. Nonlinearity and significant energy dissipation arise from the friction at the joint interfaces between these structures which can be characterized in two regimes: microslip and macroslip. Microslip of the joint occurs when an applied load causes low pressure regions of the contact interface to slip while the majority of the joint remains stuck. This region presents a change in the effective modal damping and natural frequency as a function of vibrational amplitude, i.e. leading to weakly nonlinear systems. As the joint is further loaded, macroslip occurs when the entire contact interface exhibits slip which is characterized by complicated phenomena such as modal coupling and multi-harmonic responses, and even joint failure.

Although finite element software can solve contact problems with high fidelity with friction elements such as Coulomb friction and capture microslip behavior [1], it requires significant mesh refinement and large mesh densities at the interfaces in order to obtain an accurate predictive model. Jewell, et al. [2] demonstrated this using a commercial finite element package (Abaqus®) where models with one or two joints were studied; her results showed showed that, in order to accurately simulate the static response, the mesh needed to be highly refined and

much effort was needed to find an appropriate set of solver settings. This required tens of hours of simulation per iteration and considerable effort to obtain reasonable solutions. Extrapolating this method to realistic systems with 100s to 1000s of joints and to cases where the dynamic response must be computed over many cycles (whereas Jewell et al. modeled only a quarter vibration cycle), it is clear that modeling the contact in detail is not feasible.

In industry, the common approach to modeling joints is to spider each joint interface together using multi-point constraints (MPCs) [3] to reduce each contact surface down to a single point and apply either linear springs for a linear analysis or a combination of springs and hysteretic elements to capture nonlinear behavior [4, 5] as shown in Fig 1.

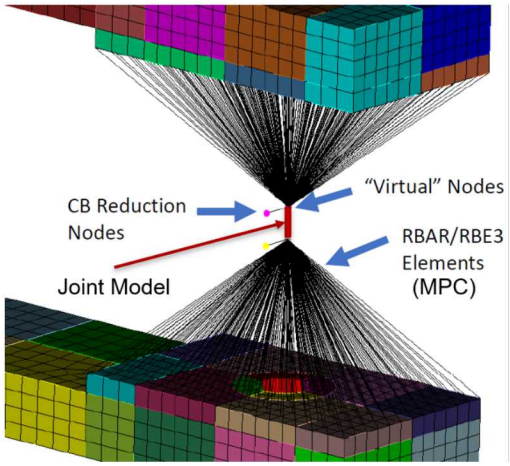


**FIGURE 1**: A schematic of a spidered model where two interfaces are reduced to a single node and connected via a whole joint model [6]

These constraints are meant to approximate the actual contact, where in reality there are certain regions in the interface that have adequate pressure to remain fully in contact (i.e. stuck). In other regions, the material may have no contact stiffness due to gapping or may switch between opened and closed as the structure vibrates. Lacayo and Allen [7] used MPCs alongside a whole-joint hysteretic Iwan Model [8] and Quasi-Static Modal Analysis (QSMA) [9] to determine the amplitude dependency of the modal properties by iterating on the Iwan parameters used to model the joint interface. They observed pareto fronts which gave a trade off where either the frequency error or damping error between numerical/experimental results could be minimized, but not both. Singh et al. [6] showed that this spidering approach yields different results depending on whether the spiders were rigid (i.e. RBAR) or averaging type (i.e. RBE3) and the size of the contact area. The RBAR MPC was shown to be the most effective at matching the experimental data, with all but one of the models, it was impossible to obtain a good fit to measurements.

This work seeks to develop an alternative that transitions from the traditional MPC approach to a continuous flexible interface and inherently extend linear reduction techniques to nonlinear problems. To do so, a full FEM is reduced down to the interface DOF using a Hurty/Craig Bampton (HCB) reduction to decrease the size of the model. Then a preload is applied using the penalty stiffness method shown by Hughes et. al. [10] to generate a preloaded model with friction that would capture the response at low amplitudes when the joints are fully stuck and a preload model without friction to represent the system when the joints are fully slipping yet still in contact. The nonlinear interface portion of these two models were then reduced using System Level Characteristic Constraint (S-CC) reduction to obtain a subset of interface deformation shapes [11]. In the reduced S-CC space, a physical Iwan element is added to each S-CC DOF to approximate the nonlinearity localized at the interface. This allows for the nonlinear hysteretic model to be applied in a decoupled coordinate space while potentially preserving the coupling between modes when the nonlinear interface forces are projected onto the structure's linearized modes. This method differs from a Modal Iwan approach [**?**] since modal Iwan cannot capture modal coupling due to the formulation, but still significantly captures the effects of many joints simultaneously.

This work evaluates the ability of this new S-CC method to capture the nonlinear behavior of various modes of a simple 2D beam structure. The performance of this approach is also compared to a traditional approach where the interface nodes are spidered using rigid bar elements (RBAR) and connected through an Iwan joint, as in [6, 7]. It begins to address the concern of the variation in results with the spidered models, by reducing the model to a set of DOF in the modal domain while maintaining the flexibility of the interface (no rigid or averaging constraints).

## THEORY AND METHODOLOGY

### Hurty/Craig Bampton Reduction

Consider an undamped equation of motion for a multi degree of freedom system as given by Eq. 1, where $\mathbf{M}$ is the mass matrix, $\mathbf{K}$ is the stiffness matrix, $F$ is the external forcing, $F_J(u,\theta)$ is the source of the nonlinearity, u is the physical displacement, and $\ddot{u}$ is the physical acceleration. If the nonlinear force is only applied to a boundary, a Reduced order model (ROM) can be used to approximate the full-order model at that set of reduction nodes [12]. Although many methods of model reduction exist, this paper will focus on the HCB method as discussed in [13].

$$\mathbf{M}\ddot{u} + \mathbf{K}u + F_J(u,\theta) = F \tag{1}$$

For the HCB method, the system is partitioned between the boundary and internal DOFs as

$$\begin{bmatrix} \mathbf{M}_{ii} & \mathbf{M}_{ib} \\ \mathbf{M}_{bi} & \mathbf{M}_{bb} \end{bmatrix} \begin{Bmatrix} \ddot{\mathbf{u}}_i \\ \ddot{\mathbf{u}}_b \end{Bmatrix} + \begin{bmatrix} \mathbf{K}_{ii} & \mathbf{K}_{ib} \\ \mathbf{K}_{bi} & \mathbf{K}_{bb} \end{bmatrix} \begin{Bmatrix} \mathbf{u}_i \\ \mathbf{u}_b \end{Bmatrix} + \begin{Bmatrix} 0 \\ \mathbf{F}_{j,b(\mathbf{u}_b)} \end{Bmatrix} = \begin{Bmatrix} 0 \\ \mathbf{F}_b \end{Bmatrix} \tag{2}$$

where subscripts $b$ and $i$ represent the boundary and interior DOF respectively. Note that only the boundary DOF are assumed to be forced either externally or internally through the joint. The interface is described by static constraint modes. The interior is described by vibration modes (fixed-interface modes) and the static constraint modes. These are combined to capture the dynamics joined full structure. As a result, a small number of fixed interface modes, $\Phi$, are computed and that basis is augmented with constraint modes, $\Psi$, as detailed [14], to obtain the HCB transformation matrix,

$$\begin{Bmatrix} \mathbf{u}_i \\ \mathbf{u}_b \end{Bmatrix} = \mathbf{T}^{\text{HCB}} \begin{Bmatrix} \mathbf{q}_i \\ \mathbf{u}_b \end{Bmatrix} = \begin{bmatrix} \Phi & \Psi \\ \mathbf{0} & \mathbf{I} \end{bmatrix} \begin{Bmatrix} \mathbf{q}_i \\ \mathbf{u}_b \end{Bmatrix} \tag{3}$$

This transformation then reduces the equations of motion to the following where the bar above the mass and stiffness terms indicates the transformed HCB model,

$$\begin{bmatrix} \mathbf{I} & \bar{\mathbf{M}}_{ib} \\ \bar{\mathbf{M}}_{bi} & \bar{\mathbf{M}}_{bb} \end{bmatrix} \begin{Bmatrix} \ddot{\mathbf{q}}_i \\ \ddot{\mathbf{u}}_b \end{Bmatrix} + \begin{bmatrix} \Lambda_{ii} & \mathbf{0} \\ \mathbf{0} & \bar{\mathbf{K}}_{bb} \end{bmatrix} \begin{Bmatrix} \mathbf{q}_i \\ \mathbf{u}_b \end{Bmatrix} + \begin{Bmatrix} 0 \\ \mathbf{F}_{j,b}(\mathbf{u}_b) \end{Bmatrix} = \begin{Bmatrix} 0 \\ \mathbf{F}_b \end{Bmatrix} \tag{4}$$

The ROM can be used to analyze the dynamic response of a structure more efficiently than the full finite element model, depending on the number of boundary DOF that must be retained in the nonlinear internal force vector. The quasi-static HCB model is solved for the preloaded equilibrium state as,

$$\begin{bmatrix} \Lambda_{ii} & \mathbf{0} \\ \mathbf{0} & \bar{\mathbf{K}}_{bb} \end{bmatrix} \begin{Bmatrix} q_i \\ u_{pre} \end{Bmatrix} + \begin{Bmatrix} 0 \\ \mathbf{F}_{j,b}(\mathbf{u}_{pre}) \end{Bmatrix} = \begin{Bmatrix} 0 \\ \mathbf{F}_{pre} \end{Bmatrix} \tag{5}$$

The joint force, $\mathbf{F}_{j,b}(\mathbf{u}_{pre})$, is modeled here using the node-to-node penalty stiffness method using either normal gap elements or triaxial gap elements. The former only applies penalty stiffness in the direction normal to the contact surface, whereas the triaxial spring applies additional in-plane stiffness when a contact gap closes. Consider the jth node pair, such that the normal gap is computed as,

$$g^j = (Z_2^j - \Delta Z_2^j) - (Z_1^j - \Delta Z_1^j) \tag{6}$$

where Z is the undeformed normal coordinate of each and $\Delta Z$ is the relative normal displacement. $\Delta Z$ is the amount of displacement present during the preload step. The penalty spring method defines the normal contact force for the jth node pair as,

$$F_Z^j = \begin{cases} k_z g^j & g^j < 0 \\ 0 & g^j \geq 0 \end{cases} \tag{7}$$

The normal penalty spring stiffness is denoted as $k_z$. For the triaxial penalty spring, an in-plane stiffness term is included, with in-plane penalty stiffnesses $k_x$ and $k_y$,

$$F_X^j = \begin{cases} k_x \Delta X^j & g^j < 0 \\ 0 & g^j \geq 0 \end{cases} \tag{8}$$

$$F_Y^j = \begin{cases} k_y \Delta Y^j & g^j < 0 \\ 0 & g^j \geq 0 \end{cases} \tag{9}$$

The joint force, $\mathbf{F_J}(\mathbf{u})$ is created by assembling the $F_X$, $F_Y$, $F_Z$ for all of the nodes at the interface. This is done in lieu of a friction element like Coulomb or Jenkins for the in-plane directions. This avoids having to compute stick/slip states for closed elements, and is a simplified contact element to be able to capture the approximate contact area in the joint, not necessarily to capture the frictional damping. Following the quasi-static preload analysis of the model in Eq. 4, the model is linearized about this equilibrium state yielding,

$$\begin{bmatrix} \mathbf{I} & \bar{\mathbf{M}}_{ib} \\ \bar{\mathbf{M}}_{bi} & \bar{\mathbf{M}}_{bb} \end{bmatrix} \begin{Bmatrix} \ddot{q}_i \\ \ddot{u}_b \end{Bmatrix} + \begin{bmatrix} \Lambda_{ii} & \mathbf{0} \\ \mathbf{0} & \bar{\mathbf{K}}_{bb} + \left.\frac{\partial \mathbf{F_j}}{\partial \mathbf{u_b}}\right|_{\mathbf{u_{pre}}} \end{bmatrix} \begin{Bmatrix} q_i \\ u_b \end{Bmatrix} = \begin{Bmatrix} 0 \\ \mathbf{F}_b \end{Bmatrix} \tag{10}$$

The partial derivative of the nonlinear force added to the HCB stiffness matrix at the boundary DOF represents the stiffness of the joint in either a fully stuck state in the case of the triaxial penalty spring, or a fully slipped state for the normal penalty springs.

### System Level Characteristic Constraint Reduction (S-CC)

The application of the System Level Characteristic Constraint (S-CC) interface reduction further decreases the number of DOF in the Hurty/Craig-Bampton ROM in Eq. 10. This approach computes the eigenvectors from the boundary partition of

the linearized HCB model and uses a truncated set of the S-CC modes as a basis for the reduction [11, 14]. The modes are computed about the linearized state, and the subscript CC denotes characteristic constraint modes,

$$\left(\mathbf{K}_{bb}+\left.\frac{\partial \mathbf{F}_j}{\partial \mathbf{u}_b}\right|_{\mathbf{u_{pre}}}-\omega_{cc}^2\mathbf{M}_{bb}\right)\Phi_{cc}=\mathbf{0} \tag{11}$$

Depending on the type of penalty springs used to linearize the system, this equation produces either the fully stuck or fully slipping S-CC modes. A truncated subset of the S-CC modes is used to further reduce the HCB mass and stiffness matrices using the transformation matrix,

$$\mathbf{T}_{SCC}=\begin{bmatrix}\mathbf{I} & \mathbf{0}\\ \mathbf{0} & \Phi_{cc}\end{bmatrix} \tag{12}$$

$$\mathbf{M}_{SCC}=(\mathbf{T}_{SCC})^T\begin{bmatrix}\mathbf{I} & \bar{\mathbf{M}}_{ib}\\ \bar{\mathbf{M}}_{bi} & \bar{\mathbf{M}}_{bb}\end{bmatrix}\mathbf{T}_{SCC} \tag{13}$$

$$\mathbf{K}_{SCC}=(\mathbf{T}_{SCC})^T\begin{bmatrix}\Lambda_{ii} & \mathbf{0}\\ \mathbf{0} & \bar{\mathbf{K}}_{bb}+\left.\frac{\partial F_j}{\partial u_b}\right|_{u_{pre}}\end{bmatrix}\mathbf{T}_{SCC} \tag{14}$$

If all CC modes are kept in the reduction, the S-CC model is identical to the HCB reduced model. This reduction method captures both the motion of the boundary and the global dynamics of the structure, resulting in a reduction of the HCB model. Utilizing the linearized EOM from the preloaded state in Eq. 10, the EOM for the S-CC reduced model about the nonlinear preloaded state is,

$$\begin{bmatrix}\mathbf{I} & \bar{\mathbf{M}}_{ic}\\ \bar{\mathbf{M}}_{ci} & \mathbf{I}\end{bmatrix}\begin{Bmatrix}\ddot{q}_i\\ \ddot{q}_{cc}\end{Bmatrix}+\begin{bmatrix}\Lambda_{ii} & \mathbf{0}\\ \mathbf{0} & \Lambda_{cc}\end{bmatrix}\begin{Bmatrix}q_i\\ q_{cc}\end{Bmatrix}=\bar{\mathbf{f}}(\mathbf{t}) \tag{15}$$

where the c subscript indicates the reduction using CC modes. The stiffness matrix is completely decoupled with $\Lambda_{cc}$, a diagonal matrix with the $\omega_{cc}^2$ values. All coupling is through the mass matrix off-diagonal terms, $\mathbf{M}_{ic}$ and $\mathbf{M}_{ci}$.

### Adding the S-CC Iwan Element

A traditional interface reduction has a set of vectors describing the motion of a top surface and a second set for the bottom surface. The S-CC model presented here is different in that it is a reduction applied after assembly. Deformations of the interface are captured by the coordinates $\mathbf{q}_c c$, whereas motions of the structure away from the interface are captured by $\mathbf{q}_i$. Hence, one can capture friction in the joint by applying a 4-parameter Iwan element between each $\mathbf{q}_c c$ coordinate and ground in Eq. 15. In this way the joint is inactive if the structure vibrates in a fixed-interface mode (with no deformation of the interface) and is activated when the interface deforms.

In the case where the joint is modeled as a normal penalty spring (i.e. fully slipped), the bolts are the only source of in-plane stiffness, and the linearized natural frequency for the ith S-CC mode shape is denoted as $\omega_{cc,i,\infty}^2$ which are the values on the diagonal of $\Lambda_{cc}$ in Eq. 15. Conversely, when the interface is fully stuck, the linearized frequency is $\omega_{cc,i}^2$. The relationship between these two models can be explicitly shown with the EOM for the S-CC coordinates. The quasi-static model of Eq. 15 appended with an Iwan element to the ith S-CC coordinate in Eq. results in,

$$\omega_{cc,i,\infty}^2 q_{cc,i}+\bar{f}_{cc,i}(q_{cc,i})=\bar{f}_i(t) \tag{16}$$

where $\bar{f}_{cc,i}(q_{cc,i})$ is the nonlinear joint model applied to the ith S-CC coordinate. The modal Iwan joint has a linearized stiffness associated with it, termed $K_T$, which can be chosen such that $\Lambda_{cc}|_i=\omega_{cc,i,\infty}^2+K_T$. This constraint is placed on the selection such that the modes 1.) converge to the fully stuck solution at low response amplitudes, and 2.) converge to the fully slipped solution at high response amplitude as the stiffness of the modal Iwan element goes to zero. In this approach, the interface DOF may be reduced while maintaining flexibility in the boundary DOF and spanning all the possible joints in the structure. It is important to note that the slipped and stuck models have different S-CC shapes and frequencies thus requiring that one augment the slipped model and its S-CC shapes with $K_T$ such that the stiffness matches that of the stuck model. The resulting nonlinear equations-of-motion with grounded S-CC modal Iwan elements becomes,

$$\begin{bmatrix}\mathbf{I} & \bar{\mathbf{M}}_{\mathbf{ic}}\\ \bar{\mathbf{M}}_{\mathbf{ci}} & \bar{\mathbf{M}}_{\mathbf{cc}}\end{bmatrix}\begin{Bmatrix}\ddot{\mathbf{q}}_{\mathbf{i}}\\ \ddot{\mathbf{q}}_{\mathbf{cc}}\end{Bmatrix}+\begin{bmatrix}\Lambda_{ii} & \mathbf{0}\\ \mathbf{0} & \Lambda_{cc,\infty}\end{bmatrix}\begin{Bmatrix}\mathbf{q}_{\mathbf{i}}\\ \mathbf{q}_{\mathbf{cc}}\end{Bmatrix}+\begin{Bmatrix}\mathbf{0}\\ \bar{\mathbf{f}}_{\mathbf{cc}}(\mathbf{q}_{\mathbf{cc}})\end{Bmatrix}=\bar{\mathbf{f}}(\mathbf{t}) \tag{17}$$

For this paper, the S-CC model with a nonlinear joint is referred to as nSCC.

### Whole Joint Models

Segalman's 4-parameter Iwan element considered both analytical solutions for contact and empirical evidence that showed

that joints exhibit power-law energy dissipation versus force (or vibration amplitude) [8]. An Iwan element is a collection of slider or Jenkins elements in parallel, in which the slip force[1] for each slider is governed by several parameters, i.e. the friction coefficient, normal force, etc.... Segalman's model recognizes that the net effect of all of these parameters must be to produce power-law dissipation versus vibration amplitude, which is now governed by only two of the four parameters in the Iwan model. The other two parameters control the transition to macroslip when the joint slips completely. Macroslip is typically not observed in engineered joints if they are tightened properly, except perhaps under extreme loading. The four parameter Iwan model can be represented by the parameters: $F_s$,$K_T$,$\chi$,and $\beta$, given in Table 1. For an in-depth discussion of the Iwan element, refer to Segalman's original paper on Iwan elements [8] and Deaner's paper on the modal Iwan model [15].

**TABLE 1**: Definition of Iwan Parameters (Physical Description)

| | |
|---|---|
| $F_S$ | The force necessary to cause macroslip |
| $K_T$ | The tangential stiffness of the Jenkins elements (i.e. the joint stiffness when no slip occurs) |
| $\chi$ | The exponent that describes the slope of the energy dissipation curve |
| $\beta$ | The ratio of the number of Jenkins elements that slip before microslip and then at macroslip |

This element is general that it can be applied physically between two interfaces for the RBAR method or between an S-CC shape and ground in the case of the nSCC ROM. The element is fundamentally the same equations, but has different interpretations of the forces (i.e. physical or modal). This enables the model to capture the hysteresis in the joint when the surface slips and generate curves that depict the amplitude dependent trends of the natural frequency and damping of the global mode. For this paper, the quasi-static method is utilized to generate these curves with the Iwan joint model. In the case of the nSCC ROM, it is important to note that adding these elements to S-CC shapes allows the modes of the system to retain some level of coupling. The reduced S-CC shapes are uncoupled, but allow coupling between different physical modes by having one shape contribute to multiple modes.

[1] If all sliders have the same friction coefficient then the slip force is defined by the normal force for each slider.

### Quasi-static Modal Analysis

The goal is to understand how each mode responds (decay and frequency of oscillation) during free vibration after a large initial force/displacement. This would require simulating the dynamic response and decomposing that into modes. However, that is computationally expensive [**?**]. The Quasi-static modal analysis method is used in lieu of a dynamic analysis to generate the hysteresis curve depicting the dependency of the modal frequency and damping ratio on amplitude. The method used is a variation to the one developed by Festjens et. al. [9] which was extended to whole joint models by Lacayo and Allen [7]. Festjens et. al. solved the quasi-static problem in which a distributed load in the shape of the vibrational mode of interest is applied on a structure at various amplitude levels. Together with Masing's rules, the load – displacement hysteresis curve yields an approximation for the dynamic response of the system. A brief overview of the method is presented here. See [7, 16, 17] for additional details and limitations. Utilizing the undamped MDOF equation of motion given in Eq. 1, at low amplitudes, the joint force $F_J(u)$ can be replaced by a low amplitude stiffness at the equilibrium position given by

$$\mathbf{K_T} = \left.\frac{\partial \mathbf{F_J}}{\partial \mathbf{u}}\right|_{\mathbf{u_0}} \tag{18}$$

The modes of the linearized system about the equilibrium point are found by solving the linearized eigenvalue problem about the preloaded state,

$$(\mathbf{K} + \mathbf{K_T} - \omega_{\mathbf{0,r}}^2 \mathbf{M})\Phi = 0 \tag{19}$$

Applying a force in the shape of the mode $\mathbf{F} = \mathbf{M}\phi_i$ where $\phi_i$ is the mode of interest, results in the following quasi-static problem where $\alpha$ are the different load levels. The acceleration term is removed since the system is solved statically.

$$\mathbf{Ku} - \mathbf{F_J}(\mathbf{u}) = (\mathbf{M})\phi_i \alpha \tag{20}$$

In this work, the nonlinear joint force comes from the Iwan element and is a function of the displacements, u. After solving Eq. 20, one obtains the static response, $u(\alpha)$, from which the modal amplitude, natural frequency, and damping ratio can be written as function of $\alpha$ as shown in Eq. 12-17 in [7]. The damping ratio is obtained by summing up the energy dissipated by friction from each Iwan joint in the system. Given that all three variables are functions of amplitude, the damping and natural frequency can be plotted in terms of modal amplitude and this is the convention that will be used in this work.

## LINEAR REDUCTION TECHNIQUES

### Structure of Interest

This work applies the S-CC Iwan reduction methodology to a 2D structure built in Abaqus, and contrasts the method using traditional MPC methods with RBAR-type elements connected with a physical four-parameter Iwan element. The 2D cantilever beam is made of steel with the properties shown in Table 2. The 2D Abaqus mesh and a diagram showing the bolt section, where a preload is applied to the top and bottom surface, and the resulting contact patch (where the nodes come into contact) is shown in Fig. 2. The beam has fixed boundary conditions on the left side of the beam for no deflection.

**TABLE 2**: Material Properties and Dimensions for the 2D Abaqus Model

| Property | Value (SI) | Value (Imperial) |
|---|---|---|
| Length | 20.32 cm | 8.00 in |
| Cross-Section | 1.27 cm square | 0.50 in square |
| Density | 7.84e-3 $kg/cm^3$ | 7.34e-4 $slinches/in^3$ |
| Elastic Modulus | 200 GPa | 2.9e7 psi |
| Poisson Ratio | 0.29 | 0.29 |

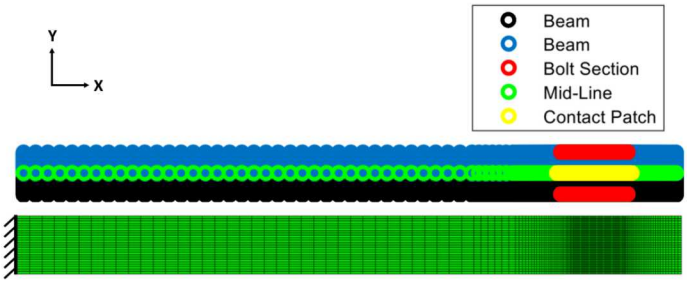


**FIGURE 2**: (Top) Node diagram of the beam, (Bottom) Abaqus beam model

The model has two beams of half the total height sandwiched to one another along the mid-line where contact occurs along the midline of ther halves. A preload distributed force is applied to the outer surfaces of the bolt section (red) and a contact simulation is done to retrieve the first six modes of the structure after preload. The resulting nodes in contact from Abaqus after preload are shown in yellow. The y direction displacement after the preload step from Abaqus for those nodes is scaled for visualization as shown in Fig. 3.

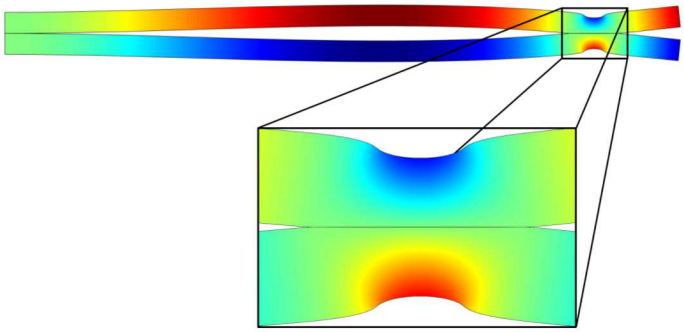

**FIGURE 3**: Scaled Y displacement of the beam after the preload step

The amplitude dependent frequency and damping curves are generated from a quasi-static analysis in Abaqus for three modes of interest: Mode 1 (first order bending), Mode 2 (second order bending), and Mode 4 (third order bending). The deformation shapes for the modes of interest are depicted in Figure 4. The mode shapes scale is exaggerated to show the shape clearly and colored by the deformation in the in-plane (x) direction.

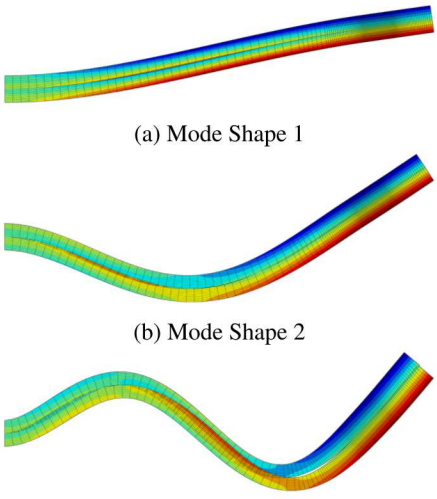

(a) Mode Shape 1

(b) Mode Shape 2

(c) Mode Shape 4

**FIGURE 4**: Stuck mode shapes of the cantilever beam for the first three modes of interest

To evaluate the effectiveness of the ROM methods, the mass and stiffness matrices from Abaqus were exported to MATLAB for the preloaded case with in-plane friction and a slipped model with no in-plane friction. It was apparently not possible to export a stiffness matrix from Abaqus that included the stiffness of any penalty springs used when solving the contact problem. Therefore to replicate those two cases, the penalty stiffness method was used in Matlab to generate the stuck and slipped model for the RBAR NLROM and the nSCC NLROM. The slipped model has only a normal spring, whereas the stuck model has a the same normal spring constant and an in-plane spring to account for friction. The nodes in contact are determined from the Abaqus preload solution. The spring constants were calibrated to minimize the frequency error between the penalty stiffness models and the frequencies from Abaqus for the slipped and stuck case. The resulting normal stiffness was 1.01e6 $lb/in$ (1.77e8 $N/m$) and the in-plane stiffness was 488.72 $lb/in$ (8.56e4 $N/m$). With these stiffnesses, the maximum error in any natural frequency (comparing the Matlab model to the natural frequencies computed by Abaqus) was 0.002%. The first six linear frequencies for the penalty stiffness model for the slipped and stuck models are given in Tab. 3. Error between the Abaqus frequencies and the penalty stiffness frequencies could be attributed to the stress straining affects present in the Abaqus solver which could perturb the results. Even with neglecting these effects, the Matlab model agrees well with the Abaqus predictions, and are suitable for developing the ROM strategy.

**TABLE 3**: Linear Frequencies for the MATLAB Slipped and Stuck Penalty Stiffness Models against Abaqus

| Mode | Slipped Model | | Stuck Model | |
|---|---|---|---|---|
| | Freq. [Hz] | Error | Freq. [Hz] | Error |
| 1 | 139.09 | 0.001% | 198.23 | 0.00% |
| 2 | 861.5 | 0.00% | 1035.8 | -0.002% |
| 3 | 1157.4 | 0.002% | 1157.4 | 0.002% |
| 4 | 2366.1 | -0.002% | 2531.6 | 0.001% |
| 5 | 3177.7 | -0.002% | 3177.7 | -0.002% |
| 6 | 4571.9 | 0.00% | 4713.6 | 0.001% |

## Linear Reduction

The full model containing 8684 DOF was reduced down to a HCB ROM of the interface of 260 interface DOF (Static Constraint Modes) and 20 Fixed Interface Modes while maintaining a maximum frequency error of 0.002% for the first 10 modes in either case. Using the HCB model, the MPC/RBAR method and S-CC Reduction were examined on their effectiveness in modeling the linear dynamics with a smaller set of DOF. The MPC/RBAR method requires that the two beams be completely uncoupled to one-another, each with their own mass and stiffness matrix. To obtain the mass and stiffness matrix of each beam at the interface, a rigid body transformation is required as given by Eq. 21 - 23 where $T_{RBAR}$ is the transformation matrix from the interface DOF to the reduced RBAR DOF, $\Psi$ are the rigid body unit deformation shapes, and $M/K_{RBAR}$ are the resulting RBAR mass and stiffness matrices.

$$\mathbf{T_{RBAR}} = \begin{bmatrix} I & 0 & 0 \\ 0 & \Psi_{RBAR,Top} & 0 \\ 0 & 0 & \Psi_{RBAR,Bottom} \end{bmatrix} \tag{21}$$

$$[\mathbf{M_{RBAR}}] = [\mathbf{T_{RBAR}}]^{\mathbf{T}}[\mathbf{M_{HCB}}][\mathbf{T_{RBAR}}] \tag{22}$$

$$[\mathbf{K_{RBAR}}] = [\mathbf{T_{RBAR}}]^{\mathbf{T}}[\mathbf{K_{HCB}}][\mathbf{T_{RBAR}}] \tag{23}$$

$\Psi$ is generated for the interface DOF for each beam by applying a unit deflection of the interface rigidly in the in-plane direction, the normal direction, and the rotation direction. The latter was calculated using $\Psi_{Rotation} = (x_{DOF} - x_c)\theta$ where $x_{DOF}$ is the location of all in-plane nodes, $x_c$ is the centroid of the interface, and $\theta$ is a unit rotation. This yields a $\Psi$ matrix of size n interface DOF for the top and bottom beams by two rigid body displacements and one rotation for each interface (total 6). As a result, the mass and stiffness matrices include 20 Fixed Interface Modes, 3 DOF for the top beam (x, y, and rotation), and 3 DOF for the bottom beam. Springs were added between each of the three DOF from the top and bottom halves of the beam to calibrate to the HCB model. Since the full/HCB models were generated with normal and in-plane springs, the slipped model was used with the expectation that a negative spring constant would be possible for the normal direction in the RBAR model to counter this constraint. Using the direct search optimization method [18] to minimize frequency error between HCB and RBAR, the following spring constants were used: $k_x = 1.95e7$ $lb/in$, $k_y = -7.88e7$ $lb/in$, and $k_\theta = -7.78e7$ $lb/in$ (3.42$e$9, $-1.38e9$, $-1.36e9$ $N/m$). The resulting frequencies against the stuck model are shown in Tab. 4.

Similar to the RBAR/MPC method, the S-CC method required 6 S-CC Shapes to correlate to the HCB reduced Model for both the slipped and stuck cases. These S-CC shapes of the

stuck case are given in Fig. 5 with the color gradient describing displacement in the x direction. The resulting frequencies for the first six modes and errors are given in Tab. 4.

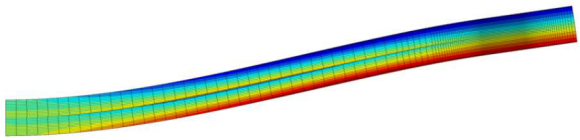

(a) S-CC Shape 1

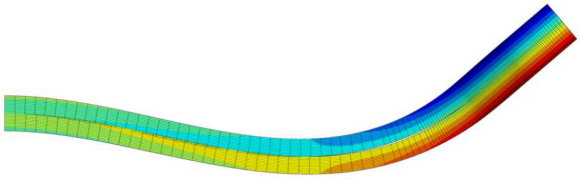

(b) S-CC Shape 2

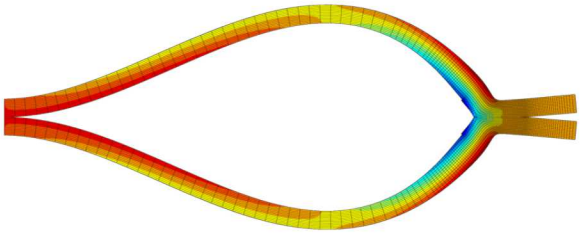

(c) S-CC Shape 3

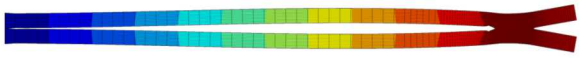

(d) S-CC Shape 4

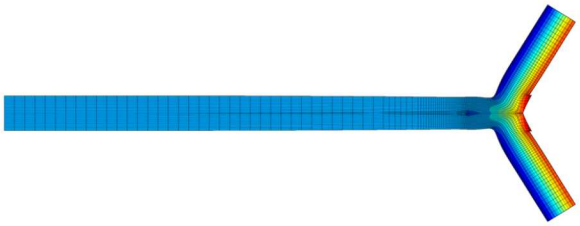

(e) S-CC Shape 5

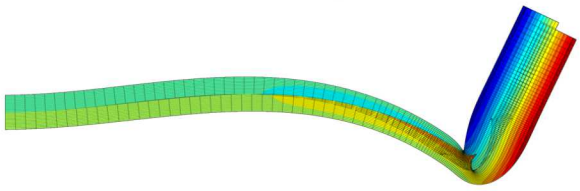

(f) S-CC Shape 6

**FIGURE 5**: S-CC Deformation Shapes

**TABLE 4**: Linear Frequencies for the Slipped Model for the HCB, RBAR, and S-CC Cases

| Mode | HCB Model Freq. [Hz] | RBAR Model Freq. Error (%) | S-CC Model Freq. Error (%) |
|---|---|---|---|
| 1 | 198.23 | -0.02 | 0.00 |
| 2 | 1035.6 | -0.03 | 0.00 |
| 3 | 1157.4 | 0.2 | 0.00 |
| 4 | 2531.6 | 0.08 | -0.001 |
| 5 | 3177.8 | -0.18 | -0.005 |
| 6 | 4717.2 | 0.30 | -0.002 |

The first few S-CC mode shapes look very similar to the first few global mode shapes of the structure. In essence, the S-CC mode shapes are the modes of a model for the complete structure after statically reducing the assembled model to the interface. However, it is also important to note that all interface DOF are free to move in the S-CC modes, so they can capture relative slip between the surfaces, as is visible in some of the higher S-CC modes. In Fig. 5, the S-CC Shapes are transformed back to the full DOF space to describe their effect on the global motion of the beam. In all 6 modes, the S-CC Reduced model produces negligible errors much lower than the RBAR reduced model. It is important to note that the reduced mode shapes for both methods remained decoupled with a max off-diagonal MAC (Modal Assurance Criterion) value of 0.48 and 0.49 for RBAR and S-CC respectively between Modes 1 and 2 [19]. The larger the off-diagonal value, the similar the mode shapes look in the reduced space. The self-MAC between the mode shapes for the Abaqus model showed the same similarity in mode shapes between Modes 1 and 2. The reductions do not increase the off-diagonal value, therefore preserving the mode shapes as present in the full model.

## NONLINEAR REDUCTION TECHNIQUES

### Nonlinear Extension of RBAR MPC Reduction

For linear analysis, three linear springs are placed between the two halves of the beams at each DOF for the RBAR approach. This is then extended to the nonlinear regime by placing an Iwan element at the DOF in the slip direction (x-direction) and linear springs elsewhere to capture the microslip of the joint of interest. This is done with the goal to compute the amplitude dependent frequency and damping curves (see Figs. 7,8) for the ROMs and compare against those obtained from Abaqus. A 100,000 itera-

tion Monte-Carlo study was conducted randomly varying $F_S$, $\gamma$, $\chi$, and $\beta$, where $\gamma$ is the scale of the linear tangential stiffness found from the relationship between the stuck and slipped S-CC stiffness matrices and given as $K_{T,Scaled} = \gamma K_T$. Furthermore, Singh et al. [6] found a correlation between a larger contact area and a reduction in the error between expected QS curves and those with an Iwan joint. To expand on this finding, this study adjusts the contact area to 0.75 and 1.5 times the nominal contact area from Abaqus. The results of the Monte-Carlo study on the three contact areas are shown in Fig. 6 for Mode 1, which depicts the RMS frequency percent error and RMS damping percent error between the RBAR nonlinear model and the Abaqus full model. The RMS error is calculated by computing the difference between the two models over the entire amplitude range of the mode. Three solutions are examined: (1) the optimal solution for the nominal contact area that minimizes frequency and damping error, (2) the solution for the larger contact area that minimizes frequency error, and (3) the solution for the larger contact area that minimizes the damping error. The frequency and damping curves for these solutions are shown Fig. 7 and 8 with the corresponding Iwan parameters in Tab. 5. It is important to note that unlike Singh, the tangential stiffness scaling is limited to $\pm 2\%$ to maintain accuracy in the linear regime. If the linear frequency error is disregarded, a better solution is possible.

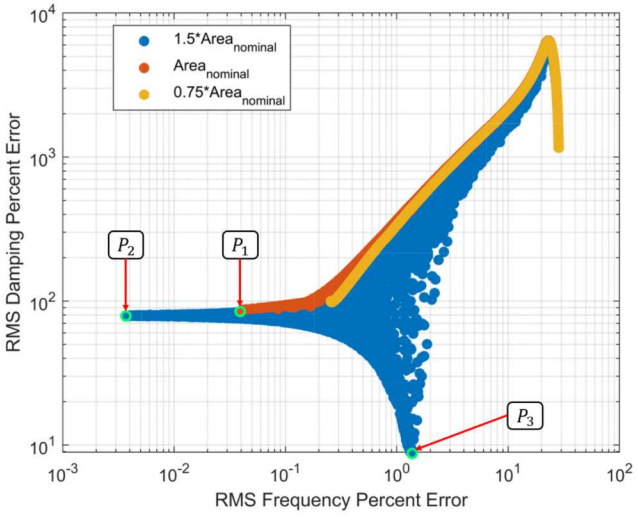


**FIGURE 6**: Mode 1 RMS frequency and damping error for a 100,000 iteration Monte-Carlo for different contact areas

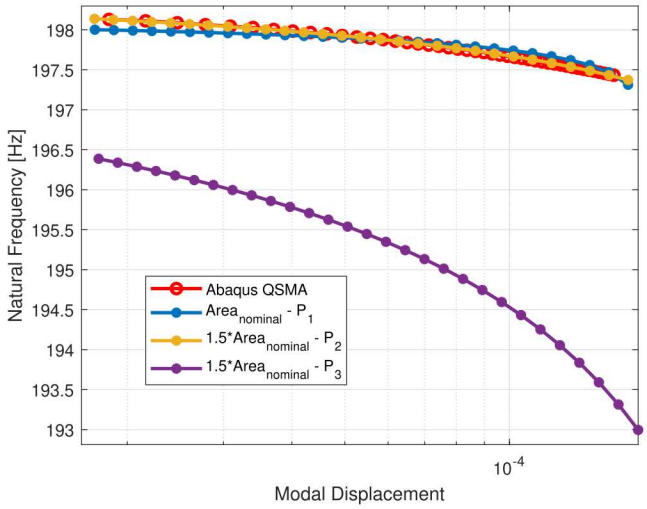


**FIGURE 7**: Mode 1 frequency vs. amplitude curve for the RBAR model vs. Abaqus

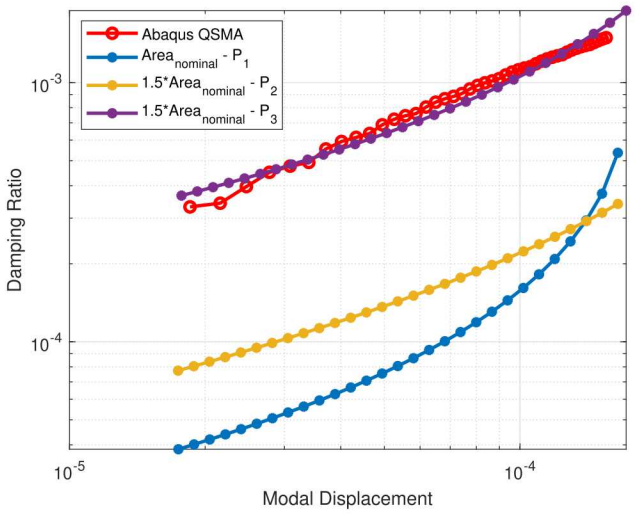


**FIGURE 8**: Mode 1 damping vs. amplitude curve for the RBAR model vs. Abaqus

**TABLE 5**: Iwan parameters for Mode 1 in the X - direction for the RBAR model

| Point | $F_S[lbf]$ | $\gamma$ | $\chi$ | $\beta$ |
|---|---|---|---|---|
| $P_1$ | 90.32 | 1.0136 | -0.892 | 0.01 |
| $P_2$ | 111.17 | 1.0072 | -0.693 | 0.585 |
| $P_3$ | 118.68 | 1.0011 | -0.8953 | 0.045 |

Increasing the contact area yielded much better results for either the frequency or damping curves, but only a small improvement in both simultaneously. The percent frequency and damping errors for the three points are shown in Table 6 clearly showing that only one modal parameter can be optimized for a given contact area within the current parameter space.

**TABLE 6**: Percent Errors for the RBAR Model against Abaqus QSMA

| Point | Contact Area | Frequency Error | Damping Error |
|---|---|---|---|
| $P_1$ | Nominal | 0.04% | 86.27% |
| $P_2$ | 1.5*Nominal | 0.003% | 78.90% |
| $P_3$ | 1.5*Nominal | 1.39% | 8.89% |

Extending the range of the $F_s$ from 1 to 50,000 did not result in curves with a lower frequency or damping error. Modes 2 and 4 could not be correlated to the Abaqus results either and, for brevity, are not shown here. In our past works we encountered similar cases, where no set of model parameters would produce a spidered model that correlated well with measurements, without sacrificing the accuracy of the linear fit, i.e. significantly changing Kt such that there was large percent error in the linear frequency. although the agreement here is worse than in any of our prior works [6].

## Proposed nSCC Method

Whereas nonlinear joint analysis in the physical domain places a hysteretic (Iwan) model between the reduced joint interfaces, this approach places an Iwan element between the ground and an S-CC modal coordinate, $\mathbf{q}_{cc}$, to capture the slip at the joint when the structure deforms in the shape of the S-CC shape in question. The eigenvectors of the S-CC reduced mass and stiffness matrices can provide insight into the contribution of each S-CC Shape on the mode of interest. Table 7 shows the percent contribution of each S-CC Shape and the 20 fixed interface modes to the three modes of interest.

**TABLE 7**: S-CC Shape Percent Contributions to the Modes of Interest

| | **Mode 1** | **Mode 2** | **Mode 4** |
|---|---|---|---|
| **Fixed Interface Modes** | 2.05 | 46.26 | 62.73 |
| **S-CC Shape 1** | 97.93 | 17.86 | 10.63 |
| **S-CC Shape 2** | 0.02 | 30.84 | 26.39 |
| **S-CC Shape 3** | 0.00 | 0.00 | 0.00 |
| **S-CC Shape 4** | 0.00 | 0.00 | 0.00 |
| **S-CC Shape 5** | 0.00 | 0.00 | 0.00 |
| **S-CC Shape 6** | 0.00 | 0.04 | 0.25 |

The results show that Mode 1 is only influenced by S-CC Shape 1, and so any nonlinearity in Mode 1 will be governed by the Iwan joint connected to S-CC Shape 1. Hence, the parameters for that Iwan joint can be determined using Mode 1 alone. In contrast, both Modes 2 and 4 are affected by S-CC Shapes 1 and 2, and so, while one might obtain initial estimates for the Iwan elements to apply at each S-CC shape using the individual modes, in the end all modes must be considered simultaneously. The $K_T$ value for each S-CC shape has already been determined as explained previously, and so this was not allowed to vary by more than 2% so as to not degrade the linear performance of the model. Similar to the RBAR model, this is done by adjusting the $K_T$ value with the scale factor, $\gamma$. Placing a 4 Parameter Iwan element at S-CC Shape 1 and updating each parameters separately until the curves overlaid, returned the following amplitude dependent frequency and damping curves for Mode 1 after the model is solved using QSMA.

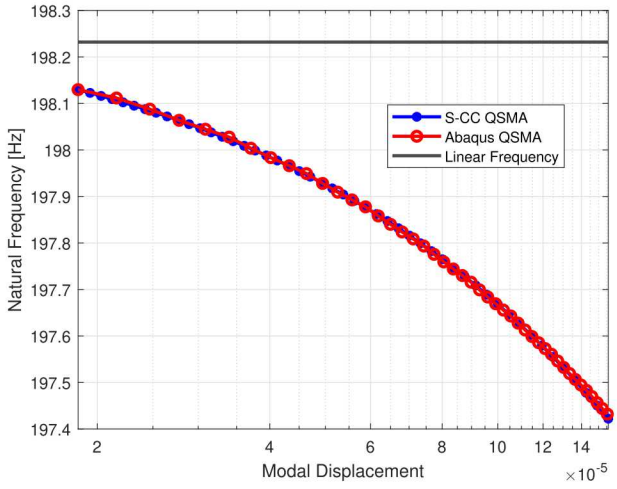


**FIGURE 9**: Mode 1 Amplitude Dependent Natural Frequency

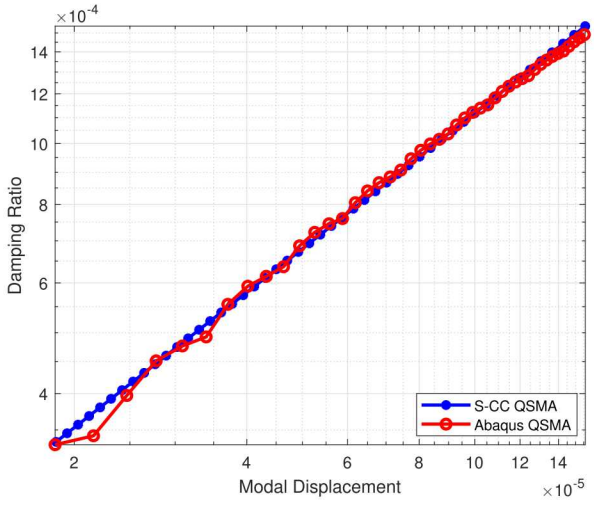


**FIGURE 10**: Mode 1 Amplitude Dependent Damping Ratio

The nSCC model can accurately capture the frequency and damping behavior of QSMA for Mode 1 with Abaqus to within 0.007% and 2.99% respectively. The fit is done simultaneously on the structure to produce these errors, whereas RBAR could fit one or the other, but not both. The larger error with damping is attributed to fitting the entire modal displacement range of the Abaqus model which does not purely exhibit power law behavior. Mode 1 can be tuned with ease since it is primarily dependent on Shape 1; however, Modes 2 and 4 require S-CC Shape 2 to be tuned to minimize the error between the S-CC and Abaqus quasi-static curves for both modes. For the purpose of the study, Modes 1 and 2, and Modes 2 and 4 were fit by fixing the parameters for S-CC Shape 1 and tuning the parameters for S-CC Shape 2. All parameters for nSCC NLROM for Modes 1 and 2 ($\text{nSCC}_{1,2}$), and Modes 1 and 4 ($\text{nSCC}_{1,4}$) are given in Table 8. In parenthesis is shown the Mode(s) to which the NLROM was tuned. Both nSCC NLROMs preserve the quasi-static response for Mode 1.

**TABLE 8**: Iwan Parameters for the two nSCC NLROMs

| **Iwan Parameters** | | | |
|---|---|---|---|
| | **S-CC Shape 1** ($M_1$) | **S-CC Shape 2** ($M_1+M_2$) | **S-CC Shape 2** ($M_1+M_4$) |
| $F_S$ | 5150 | 23481 | 16013 |
| $\gamma$ | 1.0019 | 1.0013 | 1.0000 |
| $\chi$ | -0.287 | -0.232 | -0.015 |
| $\beta$ | 0.7602 | 0.9344 | 0.12648 |

The results so far show that it is quite simple to determine the parameters for the Iwan element connected to a particular S-CC shape in order to very accurately replicate the behavior of a particular mode. However, it is usually desired to have a single NLROM to capture all of the nonlinear modes of interest. Given that both Mode 2 and 4 are dependent on Shape 2, a Monte - Carlo simulation was conducted with 100,000 iterations randomly varying $F_S$, $\gamma$, and $\chi$ for Shape 2. These parameters were bounded between the values required to calibrate $\text{nSCC}_{1,2}$ and $\text{nSCC}_{1,4}$. $\beta$ was not varied as it was the same for both models. The error metric used to find the optimal solution of the Monte - Carlo simulation is given by Eq. 24. The total error is a sum of the errors of each mode (denoted by the subscript $i$) which is found using a weighted sum of the squares of the damping and frequency errors defined by Eq. 25. Each mode can be weighted separately ($W_i$) as well as the damping and frequency ($W_\omega$, $W_\zeta$). The symbols $\omega$ and $\zeta$ refer to the damping and frequency points from QSMA respectively, and the subscript *ref* refers to the reference data, in this case the points from Abaqus quasi-static curves. The norm of these error vectors are calculated in Eq. 26 such that they can be used in subsequent equations as scalars.

$$E_{total} = (\sum E_i^2)^{1/2} \tag{24}$$

$$E_i = W_i \cdot \frac{(W_{\omega,i}^2 \cdot E_{\omega,i}^2 + W_{\zeta,i}^2 \cdot E_{\zeta,i}^2)}{\sqrt{(W_{\omega,i}^2 + W_{\zeta,i}^2)}} \tag{25}$$

$$E_{\omega,i} = \left\| ((\omega_i - \omega_{ref,i})/\omega_{ref,i}) \right\|, \quad E_{\zeta,i} = \left\| ((\zeta_i - \zeta_{ref,i})/\zeta_{ref,i}) \right\| \tag{26}$$

The optimal solution from Monte - Carlo simulation generated a single $\text{nSCC}_{1,2,4}$ that can closely reproduce the frequency and damping versus amplitude for the Abaqus truth model. Although, the curves do not overlay completely with those from Abaqus, the frequency and damping are within 0.02% and 8% of the Abaqus QSMA curves respectively for both modes. The resulting parameters for this NLROM are given in Table 9.

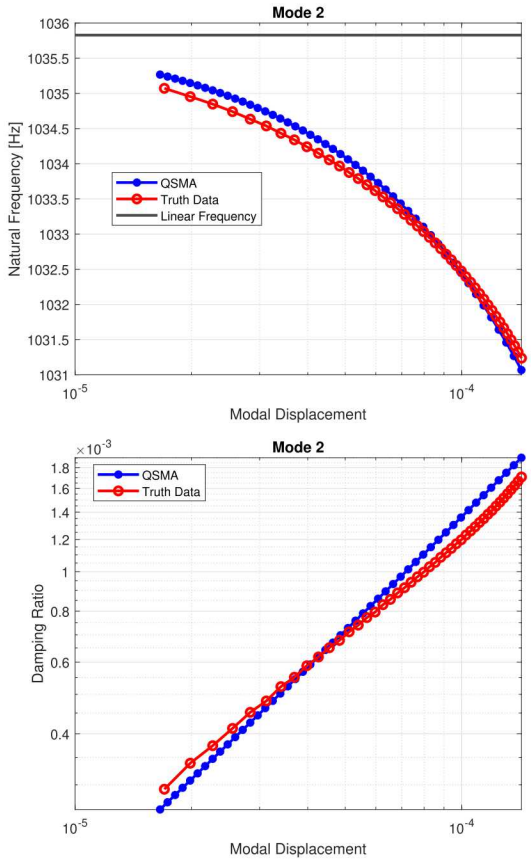


**FIGURE 11**: Mode 2 Amplitude Dependent Natural Frequency (a) and Damping (b) using nSCC $\text{ROM}_{1,2,4}$

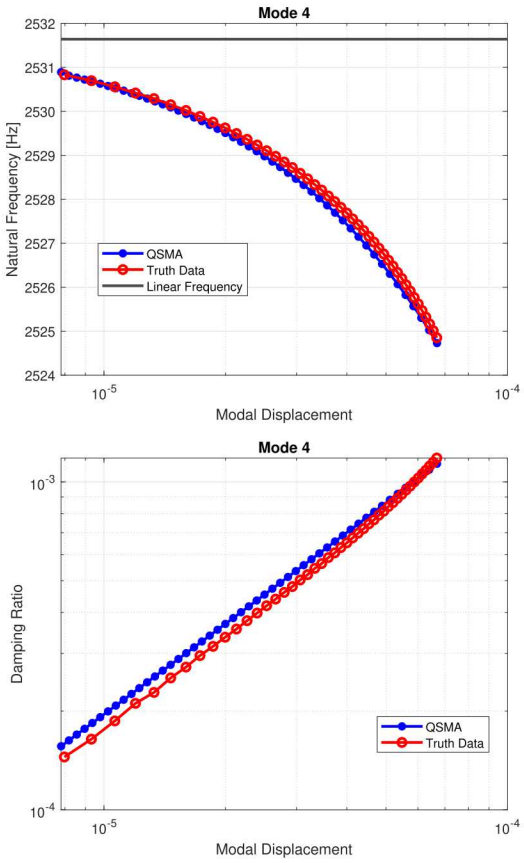


**FIGURE 12**: Mode 4 Amplitude Dependent Natural Frequency (a) and Damping (b) using nSCC $\text{ROM}_{1,2,4}$

**TABLE 9**: Iwan Parameters for the single nSCC $\text{ROM}_{1,2,4}$

| **Iwan Parameters** | | |
|---|---|---|
| | **Shape 1 (Mode 1)** | **Shape 2 (Mode 1 + Mode 2 + Mode 4)** |
| $F_S$ | 5150 | 19079 |
| $\gamma$ | 1.0019 | 1.0011 |
| $\chi$ | -0.287 | -0.0927 |
| $\beta$ | 0.7602 | 0.1026 |

A frequency weighting factor $W_\omega = 1e8$ and Mode 4 weighting factor $W_4 = 100$ were used leaving $W_\zeta$ and $W_2$ at unity. The model often chose parameters resembling those for $\text{nSCC}_{1,2}$ therefore requiring a larger weight on the error from the Mode 4

calibration. Since the damping length scale is much smaller than frequency, it is susceptible to higher errors, thus requiring a frequency weighting factor to ensure the errors are around the same order of magnitude.

## Conclusion

This paper explored the extension of linear S-CC reduction to nonlinear analyses, here dubbed as nSCC, against the traditional spidering approach with RBAR MPCs. This was done on a 2D Beam whose nonlinear frequency and damping behavior could be computed directly, in order to gauge the effectiveness of these NLROMs at recreating these curves from a high-fidelity model. The RBAR model used rigid bar constraints to reduce each interface to a single point by enforcing the same deformation, whereas S-CC reduction maintains some flexibility in the interface, depending on how many S-CC shapes are retained. The viability of both methods were evaluated on their ability to reproduce the linear natural frequencies of the beam, as well as the amplitude dependent frequency and damping curves using QSMA with Iwan joints.

The S-CC and RBAR and reduced models were able to accurately capture the linear natural frequencies of the first 6 modes of the HCB model within 0.5%. The S-CC model had errors significantly below those for RBAR. Both models needed 20 Fixed Interface Modes and 6 DOF to capture the linear dynamics by reducing the 8684 DOF in the FEM by a factor of 1000.

Iwan elements were then inserted into both models to capture the nonlinearity in the structure due to the joint. The accuracy of the models was evaluated by comparing the effective natural frequency and damping as a function of amplitude, which indicates the model's ability to more accurately predict the vibration level (and stresses) at high amplitudes when the joints are dissipating significant energy. The RBAR model was able to reproduce the frequency or damping curves for Mode 1, but not both, and the results for Modes 2 and 4 were also poor even after a thorough exploration of the parameter space. In contrast, the extension of S-CC to nonlinear (nSCC) allowed for relatively intuitive tuning of the Iwan parameters for each mode separately, and this provided initial estimates about which to center the optimization, making it far simpler. In the end, excellent correlation for the 3 modes of interest was obtained. Although Mode 3 did not exhibit nonlinearity, this model is able to capture the linear modal parameters of Mode 3. With Mode 1 dependent on Iwan parameters for S-CC Shape 1, there was a much simpler optimization problem to solve to capture the nonlinear effects of Modes 2 and 4 through S-CC Shape 2.

The S-CC reduction method performed efficiently enough on the 2D Abaqus beam to be viable for multi-joint structures. In future work we will apply the S-CC method to other models and explore whether this method can capture coupling between the modes due to the nonlinearity. The hope is that the inherent flexibility and more intuitive updating of this method will make it easier to capture the nonlinear dynamics in larger systems that exhibit more complicated phenomenon.

## ACKNOWLEDGMENT

The views expressed in the article do not necessarily represent the views of the U.S. Department of Energy or the United States Government. Sandia National Laboratories is a multimission laboratory managed and operated by National Technology & Engineering Solutions of Sandia, LLC, a wholly owned subsidiary of Honeywell International Inc., for the U.S. Department of Energy's National Nuclear Security Administration under contract DE-NA0003525.

## REFERENCES

[1] "Abaqus analysis user's guide," 2014.

[2] E. Jewell, M. S. Allen, and R. Lacayo, "Predicting damping of a cantilever beam with a bolted joint using quasi-static modal analysis," Aug. 2017.

[3] MSC.Software, "MSC Nastran 2013 Quick Reference Guide," June 2013.

[4] M. Griebel, J. Wilson, A. Johnson, B. Erickson, A. Doan, C. Flanigan, P. Bremner, J. Sills, and E. Bruno, "Orion E-STA Nonlinear Dynamic Correlation and Coupled Loads Analysis," (El Segundo, CA), June 2019. Matt Griebel, Jesse Wilson, Adam Johnson, Brent Erickson, Andrew Doan, and Chris Flanigan, Quartus Engineering, Inc., Paul Bremner, AeroHydroPLUS, Joel Sills, NASA Engineering Safety Center, Erica Bruno, Analytical Mechanics Associates, In.

[5] M. S. Allen, J. D. Schoneman, W. Scott, and J. Sills, "Leveraging Quasi-Static Modal Analysis for Nonlinear Transient Dynamics," (El Segundo, CA), June 2019.

[6] A. Singh, M. Wall, M. S. Allen, and R. J. Kuether, "Spider Configurations for Models with Discrete Iwan Elements," (Orlando, FL), 2019.

[7] R. M. Lacayo and M. S. Allen, "Updating Structural Models Containing Nonlinear Iwan Joints Using Quasi-Static Modal Analysis," *Mechanical Systems and Signal Processing*, vol. 118, no. 1 March 2019, pp. 133–157, 2019. Number: 1 March 2019.

[8] D. J. Segalman, "Model Reduction of Systems with Localized Nonlinearities," Tech. Rep. SAND2006-1789, Sandia National Laboratories, Albuquerque, NM, 2006. Issue: SAND2006-1789 SAND2006-1789.

[9] H. Festjens, G. Chevallier, and J.-L. Dion, "A numerical tool for the design of assembled structures under dynamic loads," *International Journal of Mechanical Sciences*, vol. 75, pp. 170–177, 2013.

[10] Patrick J Hughes, Wensi Wu, and Wesley E Scott, "Interface Reduction on Hurty/Craig-Bampton Substructures with Frictionless Contact," in *Nonlinear Dynamics*, vol. 1, (Orlando, FL), pp. 1–16, Springer, June 2018.

[11] M. P. Castanier, Y. C. Tan, and C. Pierre, "Characteristic constraint modes for component mode synthesis," *AIAA Journal*, vol. 39, no. 6, pp. 1182–1187, 2001. Number: 6.

[12] R. J. Kuether, P. B. Coffin, and A. R. Brink, "ON HURTY/CRAIG-BAMPTON SUBSTRUCTURING WITH INTERFACE REDUCTION ON CONTACTING SURFACES," in *International Design Engineering Technical Conferences*, (Cleveland, Ohio), 2017.

[13] R. R. J. Craig and M. C. C. Bampton, "Coupling of Substructures Using Component Mode Synthesis," *AIAA Journal*, vol. 6, no. 7, pp. 1313–1319, 1968. Number: 7.

[14] D. Krattiger, L. Wu, M. Zacharczuk, M. Buck, R. J. Kuether, M. S. Allen, P. Tiso, and M. R. W. Brake, "Interface Reduction for Hurty/Craig-Bampton Substructured Models: Review and Improvement," *Mechanical Systems and Signal Processing*, vol. 114, pp. 579–605, Jan. 2019.

[15] B. Deaner, M. S. Allen, M. J. Starr, and D. J. Segalman, "Investigation of Modal Iwan Models for Structures with Bolted Joints," Feb. 2013.

[16] M. S. Allen, R. Lacayo, and M. R. Brake, "Quasi-static Modal Analysis based on Implicit Condensation for Structures with Nonlinear Joints," Sept. 2016.

[17] R. Lacayo, B. Deaner, and M. S. Allen, "A Numerical Study on the Limitations of Modal Iwan Models for Impulsive Excitations," *Journal of Sound and Vibration*, vol. 390, pp. 118–140, 2017.

[18] J. Lagarias, J. Reeds, M. Wright, and P. Wright, "Convergence Properties of the Nelder–Mead Simplex Method in Low Dimensions," *SIAM Journal on Optimization*, vol. 9, pp. 112–147, Dec. 1998.

[19] M. Pastor, M. Binda, and T. Harčarik, "Modal Assurance Criterion," *Procedia Engineering*, vol. 48, pp. 543–548, Jan. 2012.